Nanostructured faujasite zeolite as metal ion adsorbent: kinetics, equilibrium adsorption and metal recovery studies

Mariana B. Goncalves, Djanyna V. C. Schmidt, Fabiana S. dos Santos, Daniel F. Cipriano, Gustavo R. Gonçalves, Jair C. C. Freitas and Mendelssolm K. de Pietre

ABSTRACT

The hydrothermal synthesis of nano-faujasite has been successfully performed and the effects of some crystallization parameters were investigated, along with the use of this material as a heavy-metal ion adsorbent. X-ray diffraction patterns have shown that the structure of the nano-faujasite is strongly dependent on both the crystallization time and the alkalinity of the synthesis medium. According to N_2 physisorption, X-ray fluorescence, SEM/EDS, and solid state ^{29}Si and ^{27}Al NMR data, the produced nano-faujasite consists of a solid with low molar Si/Al ratio (1.7), with high availability of ion exchange sites and high surface area/small particle size, allowing easy diffusion of metal ions to adsorbent active sites. As a consequence, an excellent performance on removal of Cd^{2+}, Zn^{2+} and Cu^{2+} ions was found for this solid. The adsorption capacity followed the order Cd^{2+} (133 $mg{\cdot}g^{-1}$) > Zn^{2+} (115 $mg{\cdot}g^{-1}$) > Cu^{2+} (99 $mg{\cdot}g^{-1}$), which agrees with the order of increasing absolute values of the hydration energy of the metal ions. Kinetic studies and adsorption isotherms showed that the metal ion removal takes place by ion exchange on the monolayer surface of the nano-faujasite. The electrochemical recovery of copper in metallic form exhibited an efficiency of 80.2% after 120 min, which suggests that this process can be adequately implemented for full-scale metal removal.

Key words | kinetics and adsorption, nano-faujasite, metal removal

Mariana B. Goncalves
Djanyna V. C. Schmidt
Mendelssolm K. de Pietre (corresponding author)
Department of Chemistry -ICEx,
Fluminense Federal University,
Rua Desembargador Ellis Hermydio Figueira, 783,
27213-145 Volta Redonda, RJ,
Brazil
E-mail: *mkpietre@yahoo.com.br*

Fabiana S. dos Santos
Department of Agribusiness Engineering,
Fluminense Federal University,
Avenida dos Trabalhadores, 420 Volta Redonda, RJ,
Brazil

Daniel F. Cipriano
Gustavo R. Gonçalves
Jair C. C. Freitas
Laboratory of Carbon and Ceramic Materials,
Department of Physics,
Federal University of Espírito Santo,
29075-910 Vitória, ES,
Brazil

HIGHLIGHTS

- Nanostructured faujasite for high metal retention.
- Considerable reusability capacity.
- Electrochemical recovery.

INTRODUCTION

The environmental contamination with heavy metals has attracted the attention of researchers worldwide because these heavy metals are not essential nutrients for the vast majority of organisms, are highly toxic and not biodegradable (He *et al.* 2016; Nagy *et al.* 2017; Sobhanardakan & Zandipak 2017; Gong & Tang 2020). The major concern is that most industrial effluents are not appropriately treated prior to their discharge (Stojakovic *et al.* 2011).

In order to minimize the effects of these contaminants, several remediation techniques are used, such as precipitation, phytoextraction, ultrafiltration and reverse osmosis. Among these methods, the use of low cost adsorbents for water treatment is promising especially when extensive heavy metals uptake take place (Sobhanardakan & Zandipak 2017).

Heavy metal removal with activated carbon can be an excellent option at first; however, due to the high cost of

doi: 10.2166/wst.2020.580

its production and regeneration, the large-scale process becomes practically unfeasible (Erden *et al.* 2004). On the other hand, the use of natural zeolites is not an interesting alternative, since neither structural pores nor chemical composition can be controlled (Perego *et al.* 2013; Oliveira *et al.* 2017). Natural solids generally contain impurities and small pore systems that can hinder the adsorption process.

In this sense, synthetic zeolites have been shown to be attractive for heavy metal removal, since their chemical and textural properties can be properly designed for adsorption processes and catalysis (Pietre *et al.* 2012; Irannajad *et al.* 2016). The use of zeolites in both catalysis and adsorption processes is favored by aspects such as: (1) high specific surface area and a 3D framework of pores with diameters compatible with the size of molecules present in substances used in many industrial processes; (2) control of the Si/Al molar ratio (Pietre *et al.* 2011). The isomorphous replacement of Si^{4+} by Al^{3+} gives rise to a framework with negative charge that is compensated by alkali or alkali earth metal cations. Therefore, an excellent performance can be expected for adsorbents with high Al content, high specific surface area and large pore sizes in ion exchange operations.

Based on this information, faujasite-type zeolites display superior performance in different segments because they have a 3D-framework comprised of large pores, high specific surface area and low Si/Al molar ratio (i.e. high Al content) when compared to other microporous solids (Nibou *et al.* 2010; Ghrib *et al.* 2016). In addition, their synthesis is carried out in the absence of organic structural directing templates, thus eliminating the calcination step at the end of the hydrothermal synthesis, which makes the process more attractive from both the economic and the environmental points of view.

Few works have reported the synthesis of nano-faujasite for applications in some important areas such as catalysis (Vuong *et al.* 2010) and adsorption processes (Humelnicu *et al.* 2017), obtaining interesting results. Smaller particles tend to display larger surface area and, therefore, more active sites may be available for adsorbate interaction with less diffusional restrictions in relation to micro-sized zeolites (Chaves *et al.* 2012).

Adsorption studies onto zeolites generally are concerned only with parameters influencing the adsorption event; that is, the effect of pH, contact time, adsorbent content, adsorbate concentration, etc. Unfortunately, the role played by the chemical and textural properties of the zeolite on the efficiency for metal removal is not frequently investigated. In addition, there are few studies that adequately deal with the recovery of the metal ions contained in the regenerated solution.

Considering the increasing importance of nanostructures for applications in environmental remediation, the present work aims to produce nano-faujasite without an organic directing template by varying the experimental conditions (i.e. the hydrothermal treatment time and the alkalinity of the synthesis reaction medium), along with the use of this material for metal ion removal from aqueous solutions. Furthermore, electrochemical deposition was used to promote the recovery of copper present in the regenerated solution. The proposed route can contribute to open new perspectives in terms of zeolite design for applications in environmental remediation, which can strongly impact the industrial segments that try to reduce environmental impacts and establish sustainable processes.

METHODS

Faujasite synthesis

The syntheses of the nano-faujasite samples were conducted starting from a gel with the following fixed molar composition: 7.8 SiO_2: Al_2O_3 : 207 H_2O: 9.4 Na_2O. Two systems were prepared from this gel: System A consists of NaOH (Dinâmica, purity >97%), sodium aluminate (Aldrich, as 50–56% Al_2O_3 and 37–45% Na_2O, purity ≥99.5%), sodium metasilicate (Dinâmica, as 27.5–29.5% SiO_2, 28–30% Na_2O and 40–50% H_2O, pure) and distilled water. The gel was aged for 24 h under constant magnetic stirring. System B was obtained by dissolving NaOH, sodium aluminate, sodium metasilicate and distilled water. Subsequently, 12.25 g of gel A was added to gel B. The resulting mixture was aged for 24 h under mechanical agitation before hydrothermal treatment at 100 °C for different crystallization times. The produced solids were washed, filtered and dried overnight in a desiccator. Also, in a second set of experiments, the effect of changing the alkalinity of the synthesis reaction medium (i.e. the NaOH amount) on the characteristics of the final products was investigated by decreasing the NaOH content in the synthesis gel by 10 and 50%, respectively.

Characterization

The zeolitic phase was characterized by X-ray diffraction (XRD) using a Shimadzu XRD600 powder diffractometer with the diffraction angle (2θ) scanned from 5 to 40° at a

scanning speed of 2° min^{-1}, with Cu-K_α radiation (40 kW, 30 mA).

The porous structure of the produced solids was analyzed by N_2 physisorption at 77 K using a Micromeritics ASAP2020 instrument. The samples were outgassed under vacuum at 150 °C for 2 h before the measurements. From the adsorption/desorption isotherms, the specific surface area (S_{BET}) was determined using the Brunauer, Emmett and Teller (BET) method (Lowell *et al.* 2004). The micropore volume (V_{MICRO}), micropore surface area (S_{MICRO}) and the external surface area (S_{EXT}) were calculated by the t-plot method. The total pore volume (V_{Total}) was directly measured from the amount of adsorbed gas at relative pressure (P/P_0) close to 1 (Lowell *et al.* 2004).

The semi-quantitative elemental analysis was performed by X-ray fluorescence spectrometry (XRF) using a Bruker S8/Tiger instrument. Scanning electron microscopy (SEM) images were recorded in a Shimadzu SSX-550 microscope, under vacuum and 15 kV acceleration voltage, equipped with an accessory for energy dispersive X-ray spectroscopy (EDS) analysis.

The local chemical environment was investigated by solid-state ^{27}Al and ^{29}Si magic angle spinning (MAS) nuclear magnetic resonance (NMR) experiments. The experiments were performed at room temperature using a Varian/Agilent VNMR 400 MHz spectrometer operating at a magnetic field of 9.4 T (^{27}Al and ^{29}Si NMR frequencies of 104.16 MHz and 79.41 MHz, respectively).

Regarding the ^{27}Al NMR experiments, single pulse excitation (SPE) experiments were conducted using a short excitation pulse with duration of 1.0 μs (corresponding to a nutation angle of ca. π/10), a recycle delay of 1.0 s and a MAS rate of 14 kHz. The spectra were obtained by Fourier transform of the free induction decays (FIDs), after accumulation of 200 transients. The frequency shifts (ppm) were externally referenced to the single resonance peak observed for an aqueous solution of $Al(NO_3)_3$. The ^{29}Si NMR spectra were obtained after accumulation of 400 transients, with an acquisition time of 0.032 s, a pulse duration of 4 μs, a recycle delay of 20 s and a MAS rate of 10 kHz; the spectra were externally referenced to tetramethylsilane (TMS), using the ^{29}Si NMR signal of kaolinite (at −91.2 ppm).

Adsorption experiments

The experiments were performed using 0.05 g of the nanofaujasite suspended in 120 mL of single metal ion aqueous solutions (containing Zn^{2+}, Cd^{2+} or Cu^{2+} ions), at the optimal pH conditions, ion concentration and contact time determined in preliminary experiments. After the uptake of the metals, solution aliquots were withdrawn in duplicate and quantified by atomic absorption spectrometry (Varian, model 55B SpectrAA). The removal efficiency (R) of the ions adsorbed at equilibrium and the adsorption capacity (q_e in mg·g^{-1}) were determined according to Equations (1) and (2), respectively.

$$R(\%) = \frac{C_0 - C_e}{C_0} \times 100 \quad (1)$$

$$q_e = \frac{C_0 - C_e}{m} \times V \quad (2)$$

where C_0 and C_e are the initial and the equilibrium concentrations (in mg·L^{-1}) of the metal ions, respectively, V is the solution volume (in L) and m is the zeolite mass (in g).

For the recording of the adsorption isotherms, a sample of 0.05 g of the zeolite was suspended in 120 mL of the single solution containing Zn^{2+}, Cd^{2+} or Cu^{2+} ions at different concentrations in the range from 20 to 160 mg·L^{-1} during 40 min. After determining the best concentration of metal uptake, kinetic studies were performed and aliquots were collected at different periods (5–120 min).

The non-linear kinetic data corresponding to the adsorption of Zn^{2+}, Cu^{2+} and Cd^{2+} ions were studied according to the pseudo-first order, pseudo-second order and intra-particle diffusion (Morris-Weber) models (Equations (3)–(5)) (Thanos *et al.* 2017), whereas the adsorption isotherm studies were investigated by Langmuir and Freundlich models in their non-linear forms (Equations (6) and (7)) (Mthombeni *et al.* 2016).

$$q_t = q_e\,(1 - e^{-K_1 \cdot t}) \quad (3)$$

$$q_t = \frac{q_e^2 \cdot K_2 \cdot t}{1 + q_e \cdot K_2 \cdot t} \quad (4)$$

$$q_t = K_{ipd} \cdot t^{0.5} \quad (5)$$

$$q_e = \frac{q_{max} \cdot K_L \cdot C_e}{1 + K_L \cdot C_e} \quad (6)$$

$$q_e = K_F \cdot C_e^{1/n} \quad (7)$$

In these expressions, q_t and q_e (both in mg·g^{-1}) are the amounts of ions adsorbed on the zeolite at any time t (min) and at equilibrium, respectively; K_1 (min^{-1}) and K_2 (g.mg^{-1}·min^{-1}) are the pseudo-first-order and pseudo-second-order rate constants of adsorption, respectively; and K_{ipd} is the rate constant of intra-particle diffusion.

Also, q_{max} is the maximum adsorption capacity ($mg \cdot g^{-1}$), K_L ($L \cdot mg^{-1}$) is the Langmuir equilibrium constant, K_F ($mg \cdot g^{-1}$) is the Freundlich constant (related to the adsorption capacity of the adsorbent) and $1/n$ is the empirical constant associated with surface heterogeneity.

From Equation (6), the dimensionless Langmuir parameter R_L can be defined, according to:

$$R_L = \frac{1}{1 + K_L \cdot C_0} \quad (8)$$

where for $0 < R_L < 1$ the adsorption process is considered favorable and for $R_L > 1$ the adsorption process is considered unfavorable (Pandey *et al.* 2015).

In order to assay the reusability of the adsorbent, regeneration studies were conducted by ion exchange of the preliminarily used nano-faujasite, for 48 h in $NaNO_3$ 2.0 mol L^{-1} solution. The solid was filtered and dried in a desiccator for 24 h before reuse.

Electrochemical experiments aimed at analyzing copper recovery were conducted on Solartron ModuLab XM ECS equipment. The working electrode was composed of a copper rod (0.5 cm^2), the counter electrode was composed of vitreous carbon and the reference electrode was a silver chloride electrode (Ag/AgCl/saturated KCl). Cyclic voltammetry (CV) measurements were performed over a potential range from 0.1 to −0.6 V vs Ag/AgCl at a scan rate of 25.0 mV s^{-1} for 120 min. The removal efficiency (R) of the recovered Cu^{2+} ions was calculated according to Equation (1).

For adsorption on competitive system studies, a sample of 0.05 g of the zeolite was suspended in 120 mL of the individual and multi-metal systems ($Zn^{2+} + Cd^{2+} + Cu^{2+}$) with approximately 40 mg L^{-1} each, at 25 °C for 40 min.

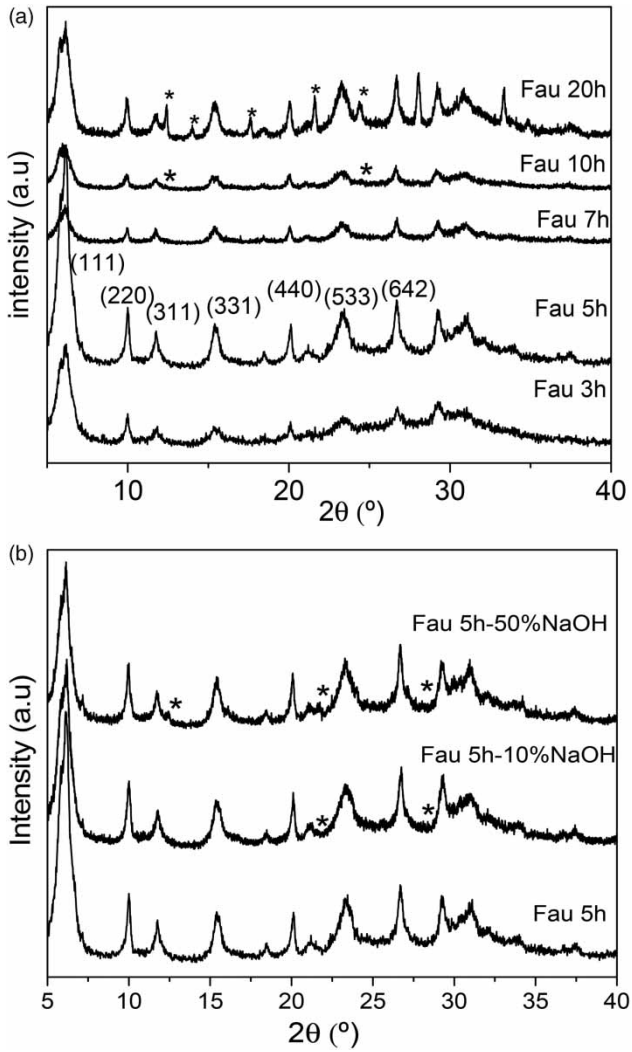

Figure 1 | XRD patterns recorded for faujasite solids prepared using different conditions: (a) samples prepared with different crystallization times; (b) effect of NaOH content. The symbol * indicates contamination with GIS phase.

RESULTS AND DISCUSSION

Characterization of the samples

The XRD patterns of the nano-faujasite samples showed only broad and weak peaks after 3 h of crystallization time (Figure 1(a)). After 5 h of crystallization, both the intensity and the sharpness of the diffraction peaks were considerably enhanced, indicating a fast crystallization rate. The XRD patterns of these two samples agree with the literature results, suggesting that the synthesized solids are single-phase faujasite (Zhan *et al.* 2002; Chaves *et al.* 2012; Zhang *et al.* 2015; Motta *et al.* 2018).

On the other hand, after 7 and 10 h of hydrothermal synthesis, an appreciable decrease in peak intensity was observed, suggesting that zeolite crystallization was complete within 5 h. Besides, the presence of XRD peaks due to the zeolite phase NaP1 (GIS type) was detected after 10 h (Chaves *et al.* 2012; Zhu *et al.* 2008). The peaks relative to this contaminant phase were more distinguishable for the solid obtained after 20 h of crystallization. Similar changes in XRD peak intensity accompanied by GIS phase formation were also reported by Zhu *et al.* (2008). Apparently, the decrease in intensity of the faujasite diffraction peaks may be related to the GIS phase transformation.

The nanocrystalline nature of the faujasite structure was evaluated from the XRD patterns shown in Figure 1, with

the average crystallite size determined according to the Scherrer equation (Muniz *et al.* 2016). The value found for the average crystallite size was 15 nm for the sample Fau 5 h, consistent with previous reports involving nano-faujasite synthesis (Zhan *et al.* 2002; Chaves *et al.* 2012). However, the particle size estimated by N_2 physisorption (D_{ext}) is around 45 nm (Table 1). The smaller value of the average crystallite size compared to the particle size is an indication of the polycrystalline nature of the zeolite particles, in agreement with previous reports (Chaves *et al.* 2012).

The XRD patterns in Figure 1(b) depict the samples produced after 5 h of hydrothermal treatment by changing the NaOH content; that is, the alkalinity. The patterns are appreciably changed after reducing the NaOH content by both 10 and 50%, where contamination with the GIS phase is observed. Based on these results, it was found that changes in both the hydrothermal treatment time and the NaOH content can lead to the formation of the GIS phase. Thus, the sample prepared with 5 h of crystallization (named Fau 5 h) was chosen for the other studies to be described in the sequence.

The particle morphology of the faujasite sample (Fau 5 h) is depicted in Figure 2(a). The SEM image reveals the presence of particles with spheroidal shape, most in the submicron size range (500–650 nm). The particle sizes observed by SEM are considerably larger than the average crystallite sizes determined by XRD, evidencing once more the polycrystalline nature of the zeolite particles. Also, EDS analyses (omitted results) show that Si, Al, O and Na are the major elements present in their chemical composition, as expected.

The Si/Al molar ratio was determined by both EDS and XRF analyses. The value obtained by EDS (1.5) was found to be close to that obtained by XRF (1.7); both these values are much smaller than the molar ratio of the synthesis gel (Table 1). Probably, due to the greater solubility of Si species in the alkaline medium, a considerable amount of these species remains dissolved in the supernatant during the crystallization process, while most Al atoms are preferably inserted into the zeolite framework (Chaves *et al.* 2012, 2015).

The N_2 physisorption isotherm of Fau 5 h sample reveals features of a type I isotherm (Figure 2(b)), typical of microporous materials, with high N_2 uptake at low

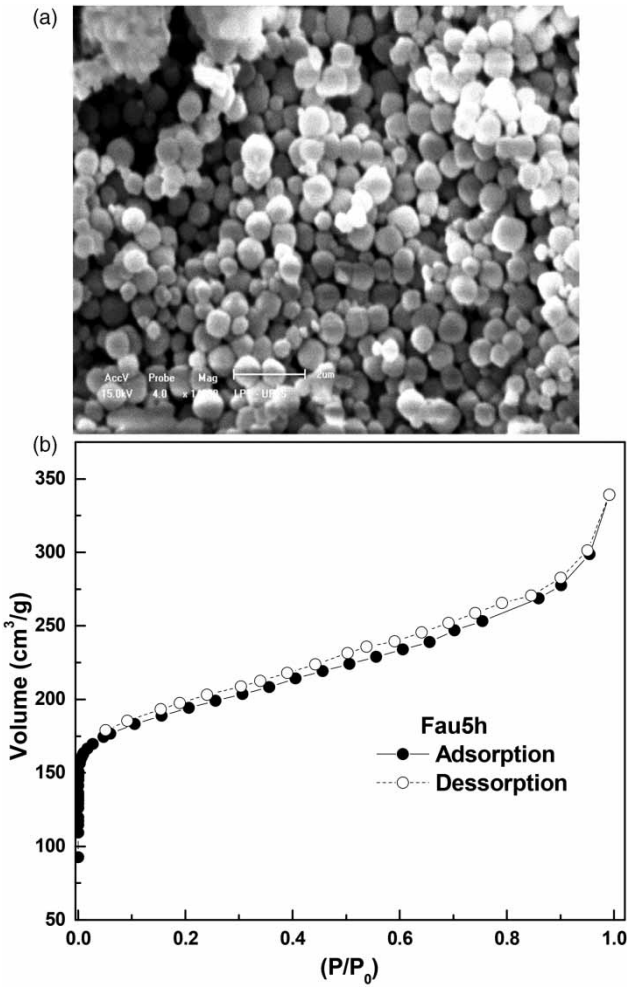

Figure 2 | SEM image, 14,000 times magnification (a) and N_2 physisorption isotherm of nano-faujasite (Fau 5 h).s

relative pressure. However, the amount of N_2 adsorbed with rising pressure is not constant, as is usually found for microporous solids due to the monolayer formation. Instead, the adsorption increases gradually with increasing P/P_0. Since this solid is essentially microporous, as can be seen in Table 1 (high S_{MICRO}), this unexpected behavior is likely to be a consequence of N_2 uptake in inter-particle voids formed by the aggregation of the particles (Zhan *et al.* 2002; Chaves *et al.* 2012; Reinoso *et al.* 2018). In addition, a H4 hysteresis loop is observed, characteristic of

Table 1 | Textural analysis results and Si/Al molar ratios for the synthesis gel (nominal composition) and final solid product (from XRF)

Sample	Si/Al_{gel}	Si/Al_{solid}	S_{BET} ($m^2 \cdot g^{-1}$)	S_{EXT} ($m^2 \cdot g^{-1}$)	S_{MICRO} ($m^2 \cdot g^{-1}$)	V_{MICRO} ($cm^3 \cdot g^{-1}$)	V_{TOTAL} ($cm^3 \cdot g^{-1}$)	D_{ext} (nm)[a]
Fau 5 h	17.6	1.7	668	90	578	0.26	0.46	45

$S_{BET} = S_{EXT} + S_{MICRO}$, S_{BET} = BET surface area, S_{EXT} = external surface area, S_{MICRO} = micropore surface area (t-plot), V_{MICRO} = micropore volume (t-plot), V_{total} = total pore volume.
[a]Calculated from the equation $D_{ext} = 4061/S_{ext}$ (Chaves *et al.* 2012).

solids containing mesopores and consisting of non-rigid aggregates of particles (Leofanti *et al.* 1998).

Regarding the textural results given in Table 1, the specific surface area and the external surface area are typical of nanostructured faujasite, which is consistent with the reduced crystallite size observed by XRD and by N_2 physisorption analysis and also in agreement with other recent reports dealing with the synthesis of nanostructured faujasites (Zhan *et al.* 2002; Chaves *et al.* 2012; Zhang *et al.* 2015).

The local arrangements of Si and Al atoms were investigated by ^{29}Si and ^{27}Al MAS NMR experiments, respectively (Figures 3(a) and 3(b)). The ^{29}Si NMR spectrum shown in Figure 3(a) reveals well-defined peaks at −81, −85 and −90 ppm, corresponding to chemical environments Si (4Al), Si (3Al) and Si (2Al), respectively; a weak shoulder is also observed, which can be described as a superposition of signals at −96 and −101 ppm, attributed to Si (1Al) and Si(0Al) species, respectively. The low-intensity signal relative to the Si (0Al) species indicates a solid with high aluminum content. The Si/Al molar ratio calculated from the ^{29}Si NMR spectra (Zhan *et al.* 2002; Motta *et al.* 2018) was 1.4, which is consistent with the results obtained by EDS and XRF analyses.

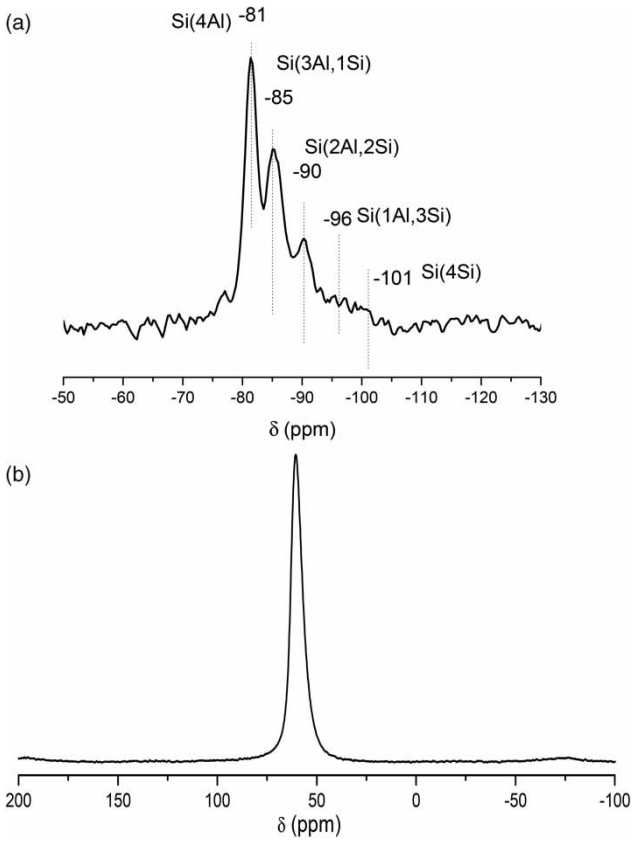

Figure 3 | Solid-state single pulse ^{29}Si MAS NMR (a) and ^{27}Al MAS NMR (b) spectra of nano-faujasite (Fau 5 h).

It is worth noting here that the presence of well-defined signals in the ^{29}Si NMR spectrum indicates a high degree of local ordering of Si atoms, contrasting with the presence of relatively broad diffraction peaks verified by XRD. Whereas XRD gives information on long-range structural ordering, the signals observed in the NMR spectra are sensitive to local ordering of atoms. Thus, the observation of broad XRD peaks and well-defined ^{29}Si NMR signals is indicative of the occurrence of a nanostructured arrangement in the nano-faujasite material.

The ^{27}Al MAS NMR spectrum obtained for the Fau 5 h sample (Figure 3(b)) is composed of an intense signal centered at 58 ppm, due to tetra-coordinated Al in the zeolitic framework (Pietre *et al.* 2012) .These structural Al sites are responsible for the negative charge in the network and, therefore, are important for ion exchange processes. The ^{27}Al MAS NMR results thus suggest that nearly all Al atoms are inserted into the nanostructure, ensuring maximum efficiency in metallic ions removal.

Thus, based on the presented characterization results, a high metal ion removal capacity by the nano-faujasite sample can be anticipated, since this material exhibits high aluminum content (i.e. low Si/Al molar ratio) and considerably large surface area and pore volume, providing a solid with high density of accessible ion exchange sites.

Adsorption experiments

Effect of initial pH

The adsorption behavior of Zn^{2+}, Cd^{2+} and Cu^{2+} ions on the nano-faujasite sample was obviously affected by the initial solution pH (Figure 4). The experiments were carried out in the pH range of 3.0–6.2. Under very acidic solutions (pH < 4.0), the great competition between H_3O^+ and metal cations for the faujasite active sites led to the lowest metal removal efficiency. In other words, both H_3O^+ and M^{2+} ions compete for the negative charge present in the zeolite framework.

Alternatively, some Al^{3+} ions may be leached out from the zeolitic framework in very acidic conditions, which reduces the availability of ion exchange sites (Moller & Bein 2013). On the other hand, both metal oxide and metal hydroxide precipitation may take place at pH values above the range used in the experiments shown in Figure 4(a), which could mask the results; thus, no adsorption experiment was performed under these conditions. The

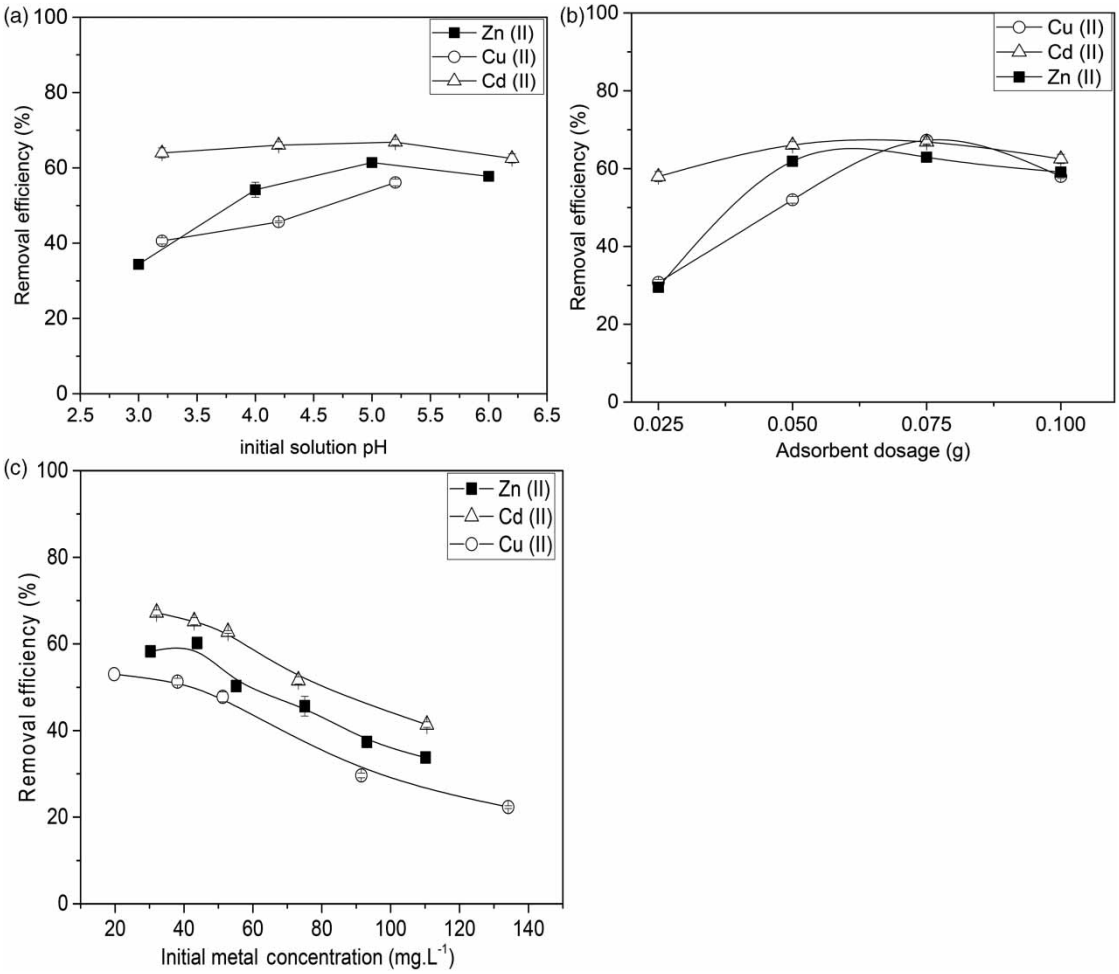

Figure 4 | Effect of initial solution pH (a), Effect of adsorbent mass (b) and initial metal ion concentration (c) on uptake of Zn^{2+}, Cd^{2+} and C^{u2+} ions by nano-faujasite (Fau 5 h). Conditions: solution volume = 120 mL; metal concentration ≈ 40 mg·L^{-1}; adsorbent mass = 50 mg; pH = 5.0 (Zn^{2+}) or 5.2 (Cd^{2+} and Cu^{2+}) and contact time = 40 min.

maximum removal efficiency was achieved at pH 5.0 (for Zn^{2+}) and 5.2 (for Cd^{2+} and Cu^{2+}), which corresponds to the pH of the as-prepared ion solutions, without further pH adjustment. In this sense, this result indicates that the electrostatic interaction between the negatively charged surface of faujasite and the metal cations is favored by using natural solution pH. Similar behavior was detected recently by our group in studies involving the uptake of cadmium, copper and zinc ions by other synthetic zeolites (Oliveira *et al.* 2017; Pratti *et al.* 2019).

Effect of adsorbent dosage

Another important parameter for identification of the optimal operating conditions in the uptake process is the amount of adsorbent, as it might influence the availability of adsorption sites. As verified in Figure 4(b), for all studied metals, an increase in the metal uptake by increasing the zeolite dosage is observed for small dosage values, due to an increased number of active sites available for adsorption. However, the amount of adsorbed metal decreases when larger amounts of the adsorbent are used. Such effect is probably associated with a decrease in the amount of available adsorption sites. This behavior may result from the electrostatic interactions, interference between binding sites, and reduced mixing at higher adsorbent densities (Çoruh *et al.* 2010). Also, particle aggregation may take place, reducing the effective surface area available for adsorption.

The maximum metal retention occurs at 50 mg of faujasite (for zinc and cadmium) and 75 mg for copper. Regarding Cu^{2+} removal, it is worth mentioning that, after the addition of 75 mg of zeolite, the solution immediately became turbid, probably due to copper hydroxide formation, as a consequence of the pH increase. Based on these results,

the most appropriate amount of adsorbent chosen for the next batch experiments of metal removal was 50 mg.

Effect of initial metal ion concentration and adsorption isotherms

Figure 4(c) displays the metal uptake on nano-faujasite as a function of initial metal ion concentration. It can be observed that the metal ion capture decreases with the increase in the solution concentration. This behavior can be attributed to the variations in the diffusion rates (driving forces to overcome the mass transfer resistance) of Cu^{2+}, Cd^{2+} and Zn^{2+} ions towards the zeolite active sites in less concentrated solutions (Pandey *et al.* 2015). The maximum removal efficiencies are observed at the lowest metal ion concentrations (20–30 $mg{\cdot}L^{-1}$), but considerable metal ion uptake is detected up to approximately 40 $mg{\cdot}L^{-1}$. Thus, an initial metal ion concentration of 40 $mg{\cdot}L^{-1}$ was chosen for the subsequent tests.

The study of equilibrium adsorption isotherms is an important tool to evaluate the adsorption capacity of a specific adsorbent. From the equilibrium adsorption data, fundamental parameters to design a practical operating procedure may be obtained. In this study, Langmuir and Freundlich models were investigated to analyze the data for the adsorption of Zn^{2+}, Cu^{2+} and Cd^{2+} ions on nano-faujasite (Fau 5 h); the adsorption data and the corresponding nonlinear fittings are shown in Figure 5 and the parameters obtained from these fittings are reported in Table 2.

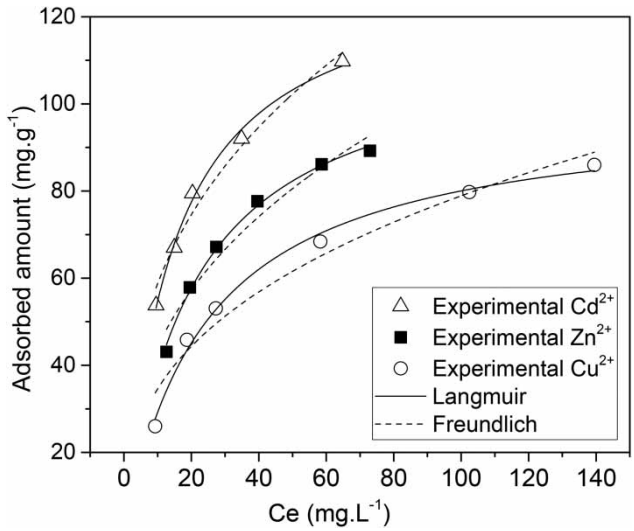

Figure 5 | Equilibrium adsorption isotherm data for the adsorption of Zn^{2+}, Cu^{2+} and Cd^{2+} ions onto nano-faujasite (Fau 5 h), with the corresponding nonlinear fittings using the Langmuir and Freundlich isotherm models.

Table 2 | Parameters obtained from the Langmuir and Freundlich models used to analyze the adsorption of Zn^{2+}, Cd^{2+} and Cu^{2+} ions onto nano-faujasite (Fau 5 h)

		Fau 5 h		
Models	**Parameter**	**Zn^{2+}**	**Cd^{2+}**	**Cu^{2+}**
Langmuir	q_{max} ($mg{\cdot}g^{-1}$)	114.6 ± 2.3	132.8 ± 3.2	99.2 ± 2.5
	K_L ($L.mg^{-1}$)	0.051	0.070	0.042
	R_L	0.099–0.489	0.050–0.324	0.043–0.180
	R^2	0.995	0.994	0.993
	RSS	5.947	8.886	4.216
Freundlich	K_F ($mg{\cdot}g^{-1}$)	18.8	26.6	15.2
	1/n	0.373	0.345	0.358
	R^2	0.950	0.970	0.952
	RSS	62.313	43.225	97.336

The coefficients of determination (R^2) associated with the Langmuir isotherm models for all studied ion metals (Table 2) were slightly higher ($R^2 \geq 0.99$) than those of Freundlich isotherm models, evidencing an adsorption of the ion metals on the zeolite via the formation of a monolayer surface. This behavior can be attributed to the fact that the nano-faujasite combines high surface area and small particle size for metal adsorption.

The faujasite structure is comprised of a supercavity whose internal diameter is approximately 1.20 nm and a pore diameter of approximately 0.74 nm (Zhang *et al.* 2013). On the other hand, the hydrated ionic radii of the divalent ions Cd^{2+} (0.429 nm), Cu^{2+} (0.419 nm) and Zn^{2+} (0.430 nm) are all smaller than these values (Álvarez-Ayuso *et al.* 2003; Ibrahim *et al.* 2010). Apparently, all of the hydrated ions can easily diffuse through the zeolite pores and channels and be adsorbed on the monolayer surface of the nano-faujasite.

The dimensionless Langmuir parameter R_L ranges from 0 to 1, which means a favorable process of adsorption of all metal ions on the nano-faujasite active sites. The value of the maximum adsorption capacity (q_{max}) is associated with the total capacity of the monolayer coverage for a given metal ion. According to Table 2, the monolayer capacity follows the selectivity sequence $Cd^{2+} > Zn^{2+} > Cu^{2+}$. This trend follows exactly the order of increasing absolute values of the hydration energy of the metal ions. In fact, Cu^{2+} ($-2{,}100\ kJ{\cdot}mol^{-1}$) and Zn^{2+} ($-2{,}044\ kJ{\cdot}mol^{-1}$) ions present the highest hydration energy absolute values, whereas Cd^{2+} ($-1{,}806\ kJ{\cdot}mol^{-1}$) ions have the lowest (Caputo & Pepe, 2007; Liu *et al.* 2019). This means that Cd^{2+} ions have less affinity to water molecules and can favorably interact with the nano-faujasite active sites more easily in relation to Cu^{2+} and Zn^{2+} ions, which tend to remain in solution.

Regarding the Freundlich parameters, $1/n$ is less than 1 in all cases, suggesting a favorable adsorption process. In addition, K_F represents the adsorption capacity on a heterogeneous surface and the values found for each metal ion indicate a high affinity for the nano-faujasite surface (Karapinar & Donat 2009).

The nanostructured faujasite sample produced in this work is thus a solid with high adsorptive capacity (q_{max}) for the removal of Cd^{2+}, Cu^{2+} and Zn^{2+} ions, when compared with some analogue systems involving different synthetic or natural zeolites (Table 3). The excellent metal uptake obtained relative to other zeolites can be understood as a consequence of: (i) low molar ratio Si/Al, which can provide high availability of ion exchange sites and (ii) high surface area and small particle size, allowing easy access of the metal ions to the nano-faujasite active sites. These features indicate the nano-faujasite sample as a feasible candidate for wastewater treatment.

Effect of contact time and kinetic studies

In order to exanimate the kinetics of the adsorption of metal ions onto nano-faujasite, three models were tested to describe the experimental data: pseudo-first order, pseudo-second order and intra-particle diffusion; the fittings are exhibited in Figure 6(a)–6(d), while the parameters obtained from these analyses are summarized in Table 4.

The plots shown in Figure 6(a)–6(c) show that the metal uptake increases rather sharply at the initial stages of adsorption (i.e. the first 0–10 min), due to the availability of active sites located on the external surface of the nano-faujasite; in the sequence, the adsorption proceeds more gradually up to 40 min, likely as a consequence of metal ions' intra-particle diffusion through the nano-faujasite pores to the inner adsorption active sites. Finally, the evidence for the full occupation of all adsorption sites can be evidenced by a plateau formation. Similar behavior has been recently observed in systems involving metal adsorption onto other aluminosilicates (Visa 2016; Oliveira *et al.* 2017). Thus, the interval of 40 min can be considered an industrially feasible period to reach the equilibrium for Cd^{2+}, Zn^{2+} and Cu^{2+} ions uptake by the nano-faujasite sample.

According to Table 4, the experimental data were better fitted by the pseudo-second order model than the pseudo-first order model, by comparing the corresponding values of the coefficients of determination (R^2). The comparison of the values of the residual sum of squares (RSS), also given in Table 4, confirms that the pseudo-second order model is the one that best fits the experimental data. This indicates that the metal ion uptake was not diffusion controlled, but instead the rate-limiting step is probably controlled by the ion exchange between the heavy metal cations and the Na^+ ions located on the zeolite surface (Pratti *et al.* 2019). Also, the q_e values obtained by the pseudo-second order model agree better with the $q_{e\ exp}$ values for all studied metal ions.

The intra-particle diffusion fittings for the metal ions uptake onto nano-faujasite are displayed in Figure 6(d), whereas Table 4 exhibits the rate constant of intra-particle diffusion (K_{ipd}) and the respective R^2 values. All the plots show a first step with a linear increase of q_t followed by a practically horizontal plateau. It is noticed that low R^2 values were found for this model.

The first step, with higher slope, corresponds to the external surface adsorption, where the metal ions diffuse through the solutions to the active sites, probably, on the external surface of the nano-faujasite sample (boundary layer diffusion) (Dinu & Dragan 2010; Stojakovic *et al.* 2011; Alver & Metin 2012). Deviations of the straight lines from the origin give an idea about the thickness of the boundary layer and are attributed to the difference in the

Table 3 | Comparative literature data on the maximum adsorption capacity (q_m) for Cd^{2+}, Cu^{2+} and Zn^{2+} ions on aluminosilicates

Aluminosilicate	Ions (single system)	q_m (mg·g^{-1})[a]	References
Faujasite-NaX	Zn^{2+} and Cd^{2+}	199 and 144	Izidoro *et al.* (2013)
Faujasite-NaX, NaA	Zn^{2+}	108 and 119	Nibou *et al.* (2010)
Faujasite nano-NaX	Cu^{2+}	126	Ansari *et al.* (2015)
Natural clinoptilolite	Zn^{2+}	21.2	Çoruh (2008)
Natural clay	Zn^{2+} and Cu^{2+}	80.6 and 44.8	Velis & Alyuz (2007)
Natural zeolite	Cd^{2+} and Cu^{2+}	25.9 and 14.3	Taamneh & Sharadqah (2017)
β-Zeolite	Cd^{2+}; Zn^{2+}; Cu^{2+}	29.5; 29.5; 17.3	Pratti *et al.* (2019)
Faujasite-NaX-from coal gangue	Cu^{2+}	45.5	Lu *et al.* (2017)
Nanostructured faujasite	Cd^{2+}; Zn^{2+}; Cu^{2+}	132.8 ± 3.2; 114.6 ± 2.3; 99.2 ± 2.5	This work

[a]q_m values derived from the Langmuir model.

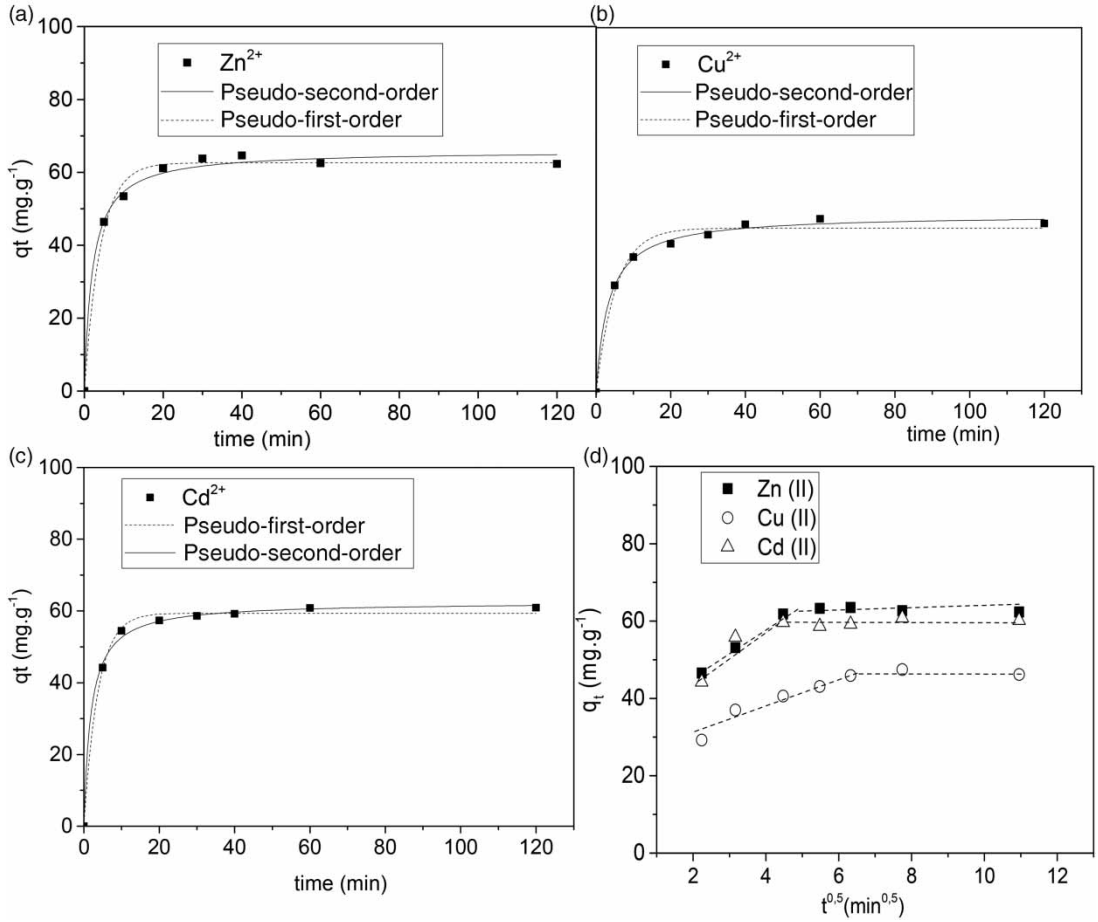

Figure 6 | Kinetic plots for metal ion adsorption onto nano-faujasite (Fau 5 h) (Figures 8(a)–8(c) = Pseudo-first-order and Pseudo-second-order fittings for Zn^{2+}, Cu^{2+} and Cd^{2+}). Figure 8(d) = intra-particle diffusion fittings for all metals studied). Conditions: adsorbent mass = 50 mg; solution volume = 120 mL; pH = 5.0 (Zn^{2+}) or 5.2 (Cd^{2+} and Cu^{2+}); metal concentration ≈ 40 mg·L^{-1}.

Table 4 | Kinetic data for the adsorption of Zn^{2+}, Cd^{2+} and Cu^{2+} ions onto nano-faujasite (Fau 5 h)

			Pseudo-first-order				Pseudo-second-order				Weber and Morris intra-particle diffusion parameters	
		$q_{e\ exp}$ mg·g^{-1}	q_e mg·g^{-1}	K_1 min^{-1}	R^2	RSS	q_e mg·g^{-1}	K_2 g.mg^{-1}.min^{-1}	R^2	RSS	K_{ipd} mg·g^{-1}.min$^{-0.5}$	R^2
Fau 5 h	Zn	64.6	62.6	0.244	0.991	4.3	65.6	0.007	0.993	3.2	1.491	0.257
	Cd	62.1	59.4	0.266	0.997	8.7	62.5	0.009	0.998	5.6	1.331	0.344
	Cu	47.1	45.0	0.189	0.982	6.2	48.7	0.006	0.996	4.5	1.816	0.617

rate of boundary layer diffusion in the initial stage of adsorption. The almost horizontal plateaus are related to intra-particle diffusion, as the final equilibrium stage is reached and the adsorption rate becomes very slow, with the observation of the maximum amount of adsorbed metal ions.

Thus, it can be verified that the external surface adsorption, observed at the first stage, is faster and also more important than the intra-particle diffusion, which occurs at the second stage. This apparently means that the intra-particle diffusion is not the only rate-limiting step, and the

adsorption process occurs through external surface adsorption and intra-particle diffusion.

Regeneration studies and electrochemical recovery

After the adsorption process, it is fundamental to be able to restore the used adsorbents for further metal ion uptake cycles. This investigation is crucial to evaluate the cost-effectiveness ratio of an adsorbent, which becomes dependent on the number of adsorption-desorption cycles that the zeolite can perform while keeping a reasonable performance (Oliveira *et al.* 2017). Batch adsorption results are expressed in Figure 7. Due to the extensive loss of adsorbent during the tests (≈15 wt. % after three reuse cycles), no more than three regeneration cycles, with similar preparations, were performed. This experiment was carried out only for Cd^{2+} and Cu^{2+} ions because of their high toxicity according to the Brazilian law (CONAMA 2011).

As can be inferred from Figure 7, the removal efficiency did not change by a considerable amount after three reuse cycles for Cd^{2+}, resulting in a reduction of approximately 12 mg·L^{-1}. However, this reduction was more pronounced for Cu^{2+}, decreasing by around 16 mg·L^{-1} after three adsorption-desorption cycles.

According to previous studies (Oliveira *et al.* 2017; Pratti *et al.* 2019), the decrease in the adsorption capacity could be explained as a consequence of the reduction in the effectiveness of the ion exchange of Na^{+} ions with Cd^{2+} and Cu^{2+} ions during regeneration in subsequent cycles. However, even if a slight decrease in the adsorption capacity of the nano-faujasite sample was found with an increasing number of cycles, this adsorbent displayed admissible reusability in the treatment of contaminated solutions containing Cd^{2+} and Cu^{2+} ions, since high metal retention is still observed, suggesting that this solid can act as a promising adsorbent for practical effluent treatment processes.

To properly dispose of the Cu^{2+} ions contained in the regenerated solution, electrochemical deposition was investigated. The cyclic voltammogram (not shown) showed a cathodic peak at −0.3 V, corresponding to the reduction of Cu (II) on the surface of the copper electrode. An efficiency of 80.2% after 120 min was achieved for the recovery of copper in metallic form. This result shows that it is feasible to recover Cu^{2+} ions and that this is a promising route for the industrial segment, which means that significant progress can be achieved and strongly impact the industrial sector to reduce environmental impacts and establish sustainable processes.

Adsorption on multi-metal system

The knowledge about multi-metal system adsorption is crucial because industrial effluents generally contain more than one kind of metal ion. Figure 8 depicts the Cd^{2+}, Cu^{2+} and Zn^{2+} ions' uptake in an individual and in a competitive system. In all cases, the adsorption capacity corresponding to each ion in a single system was found to be higher than in the multi-metal solution. This effect is

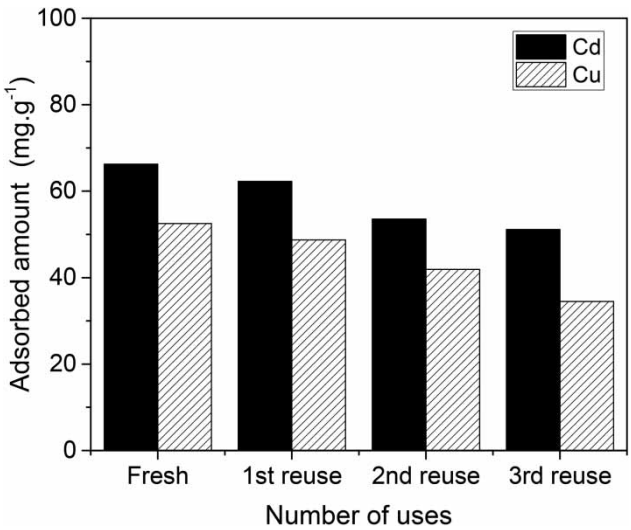

Figure 7 | Reusability experiments of adsorption of Cd^{2+} and Cu^{2+} ions onto nano-faujasite (Fau 5 h). Conditions: adsorbent mass = 50 mg; solution volume = 120 mL; pH = 5.2; metal concentration ≈ 40 mg·L^{-1}; contact time = 40 min.

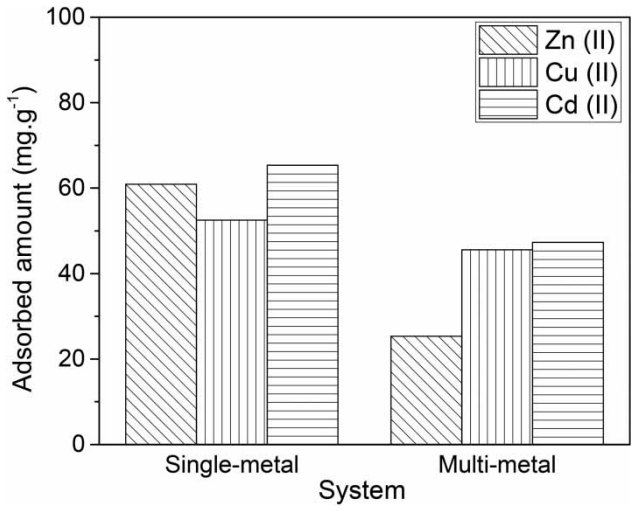

Figure 8 | Individual and multi-metal adsorption data for the adsorption of Zn^{2+}, Cd^{2+} and Cu^{2+} ions onto nano-faujasite (Fau 5 h). Conditions: adsorbent mass = 50 mg; solution volume = 120 mL; metal concentration ≈ 40 mg·L^{-1}; contact time = 40 min.

associated with the competition for the adsorption sites between the various metal ions present in the solution (Nguyen *et al.* 2015).

As stated earlier, the selective order in an individual system follows the order of increasing hydration energy absolute values of the metal ions ($Cd^{2+} > Zn^{2+} > Cu^{2+}$). However, a different behavior was observed in the case of the multi-metal system. The selectivity order in the studied multi-metal system was: $Cd^{2+} \approx Cu^{2+} > Zn^{2+}$. In this case, differently to that found for the individual systems, no direct correlation with any particular physicochemical parameter was identified and the amounts of adsorbed Cd^{2+} and Cu^{2+} ions were very close to each other. This means that, besides the hydration energy, other parameters may also be influencing the adsorption behavior of the metal ions, such as the hydrated ionic radius of the metal ions. As Cu^{2+} ions have the smallest hydrated ionic radius among the studied metals, it can be assumed that Cu^{2+} ions might have easier access to the zeolite ion exchange sites, thus leading to larger q_e values for the adsorption of Cu^{2+} ions. Thus, different behaviors are expected in single and competitive metal ion systems (Pratti *et al.* 2019).

CONCLUSIONS

The synthesis of nanostructured faujasite was successfully performed in the present work. The crystallization time of 5 h was found to be the ideal period for the formation of the nanocrystalline structure. The presence of a contaminant phase (zeolite phase NaP1, GIS type) was identified after 10 h of hydrothermal treatment. The contamination with the GIS phase was also observed after reducing the NaOH content by 10%. These results indicated that the formation of the nano-faujasite structure is strongly dependent on both the crystallization time and the alkalinity of the reaction synthesis medium. According to several characterization techniques used in this work, the produced nano-faujasite sample consists of a solid with particles in the submicron size range, high surface area, large micropore volume and low Si/Al molar ratio. These characteristics provided a solid with excellent ability to remove Cd^{2+}, Zn^{2+} and Cu^{2+} ions from aqueous solutions. According to kinetic studies and adsorption isotherms, the metal ions' uptake takes place by ion exchange on the monolayer surface of the adsorbent. The copper electrochemically recovered in metallic form showed an efficiency of 80.2% after 120 min, which is indicative that this process can be adequately used for full-scale metal removal.

ACKNOWLEDGEMENTS

The authors are grateful to FAPERJ (E-26/211.776/2015) for financial support to this work. The support from CNPq, FAPES and CAPES is also gratefully acknowledged. The authors are thankful to Dr Gilmar Clemente (UFF) for his help with the electrochemical experiments and to UFRRJ for the N_2 physisorption experiments.

AUTHORS CONTRIBUTIONS

Mariana B. Gonçalves: Investigation; **Djanyna V. C. Schmidt**: Investigation; **Fabiana S. dos Santos**: Investigation; Formal analysis; Writing – Review & Editing; **Daniel F. Cipriano**: Investigation; **Gustavo R. Gonçalves**: Investigation; Formal analysis; **Jair C. C. Freitas**: Funding acquisition; Formal analysis; Writing – Review & Editing; **Mendelssolm K. de Pietre**: Conceptualization; Funding acquisition; Formal analysis; Writing – Original Draft; Writing – Review & Editing; Project administration.

DATA AVAILABILITY STATEMENT

All relevant data are included in the paper or its Supplementary Information.

REFERENCES

Álvarez-Ayuso, E., García-Sánchez, A. & Querol, X. 2003 Purification of metal electroplating waste waters using zeolites. *Water Research* **37**, 4855–4862. https://doi.org/10.1016/j.watres.2003.08.009.

Alver, E. & Metin, A. U. 2012 Anionic dye removal from aqueous solutions using modified zeolite: Adsorption kinetics and isotherm studies. *Chemical Engineering Journal* **200-202**, 59–67. https://doi.org/10.1016/j.cej.2012.06.038.

Ansari, M., Raisi, A., Aroujalian, A., Dabir, B. & Irani, M. 2015 Synthesis of Nano-NaX zeolite by microwave heating method for removal of lead, copper, and cobalt ions from aqueous solution. *Journal of Environmental Engineering* **141** (5), 04014088-1–04014088-8. https://doi.org/10.1061/(ASCE)EE.1943-7870.0000919.

Caputo, D. & Pepe, F. 2007 Experiments and data processing of ion exchange equilibria involving Italian natural zeolites: a review. *Microporous Mesoporous Materials* **1050** (3), 222–231. https://doi.org/10.1016/j.micromeso.2007.04.024.

Chaves, T. F., Pastore, H. O. & Cardoso, D. 2012 A simple synthesis procedure to prepare nanosized faujasite crystals.

Microporous Mesoporous Materials **161**, 67–75. https://doi.org/10.1016/j.micromeso.2012.05.022.

Chaves, T. F., Pastore, H. O., Hammer, P. & Cardoso, D. 2015 As-synthesized TEA-BEA zeolite: effect of Si/Al ratio on the Knoevenagel condensation. *Microporous Mesoporous Materials* **202**, 198–207. https://doi.org/10.1016/j.micromeso.2014.09.058.

Conselho Nacional do Meio Ambiente (CONAMA) 2011 Dispõe sobre as condições e padrões de lançamento de efluentes, complementa e altera a Resolução no. 357, de 17 de março de 2005. http://www.mma.gov.br/port/conama/res/res05/res35705.pdf. (accessed 15 march 2020).

Çoruh, S. 2008 The removal of zinc ions by natural and conditioned clinoptilolites. *Desalination* **225** (1-3), 41–57. https://doi.org/10.1016/j.desal.2007.06.015.

Çoruh, S., Şenel, G. & Ergun, O. N. 2010 A comparison of the properties of natural clinoptilolites and their ion-exchange capacities for silver removal. *Journal of Hazardous Materials* **180**, 486–492. https://doi.org/10.1016/j.jhazmat.2010.04.056.

Dinu, M. V. & Dragan, E. S. 2010 Evaluation of Cu^{2+}, Co^{2+} and Ni^{2+} ions removal from aqueous solution using a novel chitosan/clinoptilolite composite: kinetics and isotherms. *Chemical Engineering Journal* **160**, 157–163. https://doi.org/10.1016/j.cej.2010.03.029Get.

Erden, E., Karapinar, N. & Donat, R. 2004 The removal of heavy metals cations by natural zeolites. *Journal of Colloid and Interface Science* **280**, 309–314. https://doi.org/10.1016/j.jcis.2004.08.028.

Ghrib, Y., Frini-Srasra, N. & Srasra, E. 2016 Synthesis of NaX and NaY zeolites from Tunisian kaolinite as base catalysts: an investigation of Knoevenagel condensation. *Journal of the Chinese Chemical Society* **63**, 601–610. https://doi.org/10.1002/jccs.201600018.

Gong, T. & Tang, Y. 2020 Preparation of multifunctional nanocomposites Fe_3O_4@SiO_2–EDTA and its adsorption of heavy metal ions in water solution. *Water Science & Technology* **81** (1), 170–177. https://doi.org/10.2166/wst.2020.099.

He, K., Chen, Y., Tang, Z. & Hu, Y. 2016 Removal of heavy metal ions from aqueous solution by zeolite synthesized from fly ash. *Environmental Science and Pollution Research* **23**, 2778–2788. https://doi.org/10.1007/s11356-015-5422-6.

Humelnicu, I., Băiceanu, A., Ignat, M. E. & Dulman, V. 2017 The removal of basic blue 41 textile dye from aqueous solution by adsorption onto natural zeolitic tuff: kinetics and thermodynamics. *Process Safety and Environmental Protection* **105**, 274–287. https://doi.org/10.1016/j.psep.2016.11.016.

Ibrahim, H. S., Jamil, T. S. & Hegazy, E. Z. 2010 Application of zeolite prepared from Egyptian kaolin for the removal of heavy metals: II. Isotherm models. *Journal of Hazardous Materials* **182**, 842–847. https://doi.org/10.1016/j.jhazmat.2010.06.118.

Irannajad, M., Haghighi, H. K. & Mohammadjafari, A. 2016 Heavy metals adsorption by nanozeolites: effect of sodium hexametaphosphate. *Environmental Earth Sciences* **75**, 1058–1064. https://doi.org/10.1007/s12665-016-5851-7.

Izidoro, J. C., Fungaro, D. A., Abbott, J. E. & Wang, S. 2013 Synthesis of zeolites X and A from fly ashes for cadmium and zinc removal from aqueous solutions in single and binary ion systems. *Fuel* **103**, 827–834. https://doi.org/10.1016/j.fuel.2012.07.060.

Karapinar, N. & Donat, R. 2009 Adsorption behavior of Cu^{2+} and Cd^{2+} onto natural bentonite. *Desalination* **249**, 123–129. https://doi.org/10.1016/j.desal.2008.12.046.

Leofanti, G., Padovan, M., Tozzola, G. & Venturelli, B. 1998 Surface area and pore texture of catalysts. *Catalysis Today* **41**, 207–219. https://doi.org/10.1016/S0920-5861(98)00050-9.

Liu, X., Tian, R., Ding, Y., He, Y. & Li, H. 2019 Adsorption selectivity of heavy metals by Na-clinoptilolite in aqueous solutions. *Adsorption* **25**, 747–755. https://doi.org/10.1007/s10450-019-00081-x.

Lowell, S., Schields, J. E., Thomas, M. A. & Thommes, M. 2004 *Characterization of Porous Solids and Powders: Surface Area, Pore Size and Density*. Kluwer Academic Publishers, Dordrecht, the Netherlands. https://doi.org/10.1007/978-1-4020-2303-3.

Lu, X., Shi, D. & Chen, J. 2017 Sorption of Cu^{2+} and Co^{2+} using zeolite synthesized from coal gangue: isotherm and kinetic studies. *Environmental Earth Sciences* **76**, 591–600. https://doi.org/10.1007/s12665-017-6923-z.

Moller, K. & Bein, T. 2013 Mesoporosity – a new dimension for zeolites. *Chemical Society Reviews* **42**, 3689–3707. https://doi.org/10.1039/c3cs35488a.

Motta, I. L., Pereira, J. G. & Cardoso, D. 2018 Properties and catalytic evaluation of nanometric X zeolites containing linear alkylammonium cations. *Molecular Catalysis* **458**, 127–138. https://doi.org/10.1016/j.mcat.2018.02.025.

Mthombeni, N. H., Mbakop, S., Ochieng, A. & Onyango, M. S. 2016 Vanadium(V) adsorption isotherms and kinetics using polypyrrole coated magnetized natural zeolite. *Journal of the Taiwan Institute of Chemical Engineers* **66**, 172–180. https://doi.org/10.1016/j.jtice.2016.06.016.

Muniz, F. T. L., Miranda, M. A. R., Santos, C. M. & Sasaki, J. M. 2016 The Scherrer equation and the dynamical theory of X-ray diffraction. *Acta Crystallographica A* **72**, 385–390. https://doi.org/10.1107/S205327331600365X.

Nagy, B., Mânzatu, C., Maicaneanu, A., Indolean, C., Lucian, B.-T. & Majdik, C. 2017 Linear and non-linear regression analysis for heavy metals removal using *Agaricus bisporus* macrofungus. *Arabian Journal of Chemistry* **10**, S3569–S3579. https://doi.org/10.1016/j.arabjc.2014.03.004.

Nguyen, T. C., Loganathan, P., Nguyen, T. V., Vigneswaran, S., Kandasamy, J. & Naidu, R. 2015 Simultaneous adsorption of Cd, Cr, Cu, Pb, and Zn by an iron-coated Australian zeolite in batch and fixed-bed column studies. *Chemical Engineering Journal* **270**, 393–404. https://doi.org/10.1016/j.cej.2015.02.047.

Nibou, D., Mekatel, H., Amokrane, S., Barkat, M. & Trari, M. 2010 Adsorption of Zn^{2+}ions onto NaA and NaX zeolites: kinetic, equilibrium and thermodynamic studies. *Journal of Hazardous Materials* **173**, 637–646. https://doi.org/10.1016/j.jhazmat.2009.08.132.

Oliveira, D. F., Neri, J. A. M., Ribeiro, J. A. A., Santos, F. S. & Pietre, M. K. 2017 Synthesis of zeolites with different chemical and textural properties for metal ions removal from aqueous solutions. *Water Science & Technology* **76** (12), 3441–3451. https://doi.org/10.2166/wst.2017.508.

Pandey, P. K., Sharma, S. K. & Sambi, S. S. 2015 Removal of lead (II) from waste water on zeolite-NaX. *Journal of Environmental Chemical Engineering* **3** (4), 2604–2610. https://doi.org/10.1016/j.jece.2015.09.008.

Perego, C., Bagatin, R., Tagliabue, M. & Vignola, R. 2013 Zeolites and related mesoporous materials for multi-talented environmental solutions. *Microporous and Mesoporous Materials* **166**, 37–49.

Pietre, M. K., Bonk, F. A., Rettori, C., Garcia, F. A. & Pastore, H. O. 2011 [V,Al]-ITQ-6: novel porous material and the effect of delamination conditions on V sites and their distribution. *Microporous and Mesoporous Materials* **1-3**, 108–117. https://doi.org/10.1016/j.micromeso.2011.04.031.

Pietre, M. K., Bonk, F. A., Rettori, C., Garcia, F. A. & Pastore, H. O. 2012 Delaminated vanadoaluminosilicate with [V,Al]-ITQ-18 structure. *Microporous and Mesoporous Materials* **156**, 244–256. https://doi.org/10.1016/j.micromeso.2012.02.032.

Pratti, L. M., Reis, G. M., Santos, F. S., Gonçalves, G. R., Freitas, J. C. C. & Pietre, M. K. 2019 Effects of textural and chemical properties of β-zeolites on their performance as adsorbents for heavy metals removal. *Environmental Earth Sciences* **78**, 553–567. https://doi.org/10.1007/s12665-019-8568-6.

Reinoso, D., Adrover, M. & Pedernera, M. 2018 Green synthesis of nanocrystalline faujasite zeolite. *Ultrasonics Sonochemistry* **42**, 303–309. https://doi.org/10.1016/j.ultsonch.2017.11.034.

Sobhanardakan, S. & Zandipak, R. 2017 Synthesis and application of $TiO_2/SiO_2/Fe_3O_4$ nanoparticles as novel adsorbent for removal of Cd(II), Hg(II) and Ni(II) ions from water samples. *Clean Technologies and Environmental Policy* **19**, 1913–1925. https://doi.org/10.1007/s10098-017-1374-5.

Stojakovic, D., Hrenovic, J., Mazaj, M. & Rajic, N. 2011 On the zinc sorption by the Serbian natural clinoptilolite and the disinfecting ability and phosphate affinity of the exhausted sorbent. *Journal of Hazardous Materials* **185**, 408–415. https://doi.org/10.1016/j.jhazmat.2010.09.048.

Taamneh, Y. & Sharadqah, S. 2017 The removal of heavy metals from aqueous solution using natural Jordanian zeolite. *Applied Water Science* **7**, 2021–2028. https://doi.org/10.1007/s13201-016-0382-7.

Thanos, A. G., Katsou, E., Malamis, S., Drakopoulos, V., Paschalakis, P., Pavlatou, E. A. & Haralambous, K. J. 2017 Cr(VI) removal from aqueous solutions using aluminosilicate minerals in their Pb-exchanged forms. *Applied Clay Science* **147**, 54–62. https://doi.org/10.1016/j.clay.2017.05.040.

Velis, S. & Alyuz, B. 2007 Adsorption of copper and zinc from aqueous solutions by using natural clay. *Journal of Hazardous Materials* **149** (1), 226–233. https://doi.org/10.1016/j.jhazmat.2007.04.109.

Visa, M. 2016 Synthesis and characterization of new zeolite materials obtained from fly ash for heavy metals removal in advanced wastewater treatment. *Powder Technology* **294**, 338–347. https://doi.org/10.1016/j.powtec.2016.02.019.

Vuong, G.-T., Hoang, V.-T., Nguyen, D.-T. & Do, T.-O. 2010 Synthesis of nanozeolites and nanozeolite-based FCC catalysts, and their catalytic activity in gas oil cracking reaction. *Applied Catalysis A* **382**, 231–239. https://doi.org/10.1016/j.apcata.2010.04.049.

Zhan, B.-Z., White, M. A., Lumsden, M., Mueller-Neuhaus, J., Robertson, K. N., Cameron, T. S. & Gharghouri, M. 2002 Control of particle size and surface properties of crystals of NaX zeolite. *Chemistry of Materials* **14**, 3636–3642. https://doi.org/10.1021/cm011635f.

Zhang, X., Tong, D. Q., Zhao, J. & Li, X. Y. 2013 Synthesis of NaX zeolite at room temperature and its characterization. *Materials Letters* **104**, 80–83. https://doi.org/10.1016/j.matlet.2013.03.131.

Zhang, X., Yang, S., Tang, D. & Yang, R. 2015 Synthesis of zeolite NaX at 25(C and 95(C: characterization, cobalt exchange and catalytic performance in epoxidation of styrene. *Materials Research* **70**, 343–347. https://doi.org/10.1016/j.materresbull.2015.04.049.

Zhu, G., Li, Y., Chen, H., Liu, J. & Yang, W. 2008 An in situ approach to synthesize pure phase FAU-type zeolite membranes: effect of aging and formation mechanism. *Journal of Materials Science* **43**, 3279–3288. https://doi.org/10.1007/s10853-008-2524-2.

First received 20 May 2020; accepted in revised form 24 November 2020. Available online 7 December 2020